Numerical method for solving stochastic differential equations with Poissonian white shot noise

Changho Kim and Eok Kyun Lee

Department of Chemistry and School of Molecular Science (BK21), Korea Advanced Institute of Science and Technology,
Daejeon 305-701, Republic of Korea

Peter Hänggi and Peter Talkner

Institut für Physik, Universität Augsburg, D-86135 Augsburg, Germany
(Received 10 May 2007; published 13 July 2007)

We propose a numerical integration scheme to solve stochastic differential equations driven by Poissonian white shot noise. Our formula, which is based on an integral equation, which is equivalent to the stochastic differential equation, utilizes a discrete time approximation with fixed integration time step. We show that our integration formula approaches the Euler formula if the Poissonian noise approaches the Gaussian white noise. The accuracy and efficiency of the proposed algorithm are examined by studying the dynamics of an over-damped particle driven by Poissonian white shot noise in a spatially periodic potential. We find that the accuracy of the proposed algorithm only weakly depends on the parameters characterizing the Poissonian white shot noise; this holds true even if the limit of Gaussian white noise is approached.

PACS number(s): 02.50.Ey, 02.60.Cb, 05.40.Ca, 05.10.−a

I. INTRODUCTION

The need for accurate simulations of stochastic processes arises across almost all disciplines of natural science, engineering, and finance. It requires not only the appropriate description of random fluctuations but also efficient numerical schemes. As a first approximation of real fluctuations with a short correlation time, Gaussian white noise (GWN) has been used almost universally. The resulting processes are described by Fokker–Planck equations [1,2] which can be tackled by analytical and numerical methods. The numerical integration of the equivalent Langevin equation offers an alternative approach for the study of stochastic processes driven by GWN [2,3].

While GWN provides an adequate description for a broad class of continuous random processes, other stochastic processes, which are also frequently met in physical, biological, chemical, and sensory systems, exhibit instantaneous discrete jumps and therefore must be modeled differently in terms of shot noise. Realizations of shot noise consist of sequences of very sharp pulses with random heights and randomly distributed times between subsequent pulses. Poissonian white shot noise (PWSN) provides a particular mathematical model of shot noise. It consists of δ-function shaped pulses, which occur at times forming a Poissonian point process. The strengths of the pulses assume identically distributed values, which are independent of each other and also independent of the times between the pulses. As a consequence of these particular properties, the autocorrelation functions and all higher multitime correlation functions of PWSN are composed of δ functions in time. This implies in particular that the power spectral density of PWSN is constant as a function of frequency. Moreover, the integral of PWSN as a function of the upper integration limit constitutes a process with independent increments. As a consequence the solutions of stochastic differential equations driven by PWSN are Markovian processes. The process remains Markovian if the noise sources are composed of GWN and PWSN [4–6]. The equations of motion of the probability

density of such processes are of first order in time and integro-differential equations in terms of the state space variables with maximally second-order derivatives. Moreover, GWN can be obtained as a limiting case of PWSN [7].

Processes driven by PWSN have been studied for various systems, such as Brownian oscillators with fluctuating parameter [8–10], or a single file of Brownian particles [11–13]. Another interesting problem is transport of Brownian particles induced by PWSN in a spatially periodic potential [14,15]. These systems may exhibit nontrivial ratchetlike transport properties even for reflection symmetric potentials. To induce a directed motion, it is essential to have nonequilibrium noise which is statistically asymmetric in the sense that its cumulants of odd order do not vanish [16,17]. Further studies include thermal ratchets driven by PWSN [18,19]. In these model systems, equilibrium thermal fluctuations are represented by GWN and nonequilibrium impulsive fluctuations by PWSN. In contrast to the above-mentioned works, which consider PWSN with pulse distributions having a finite second moment, recent work has considered pulse distributions with algebraic tails such as Pareto, or Lévy distributions [20–23].

The analytical treatment of dynamical systems driven by PWSN poses more difficulties compared to systems driven by GWN. Analytical expressions of the time-dependent probability density functions of PWSN driven processes have been derived only for very limited cases [24]. This is so because their time evolution is governed by rather intractable partial integro-differential equations [4,7,9,10,25]. Stationary solutions in the long time limit, however, are available in certain cases, for example, if the peak weights are exponentially distributed, both for natural and for periodic boundary conditions [7,14,26]. Analytical studies have been pursued for dynamical properties such as mean first-passage times or activation rates [27]. For systems driven by both GWN and PWSN, the characteristic functions of the time-dependent probability densities of jump-diffusion systems have been available in the case of constant and linear drift [28]. An

alternative approach based on the Langevin equation has been pursued for a Verhulst-type model [29].

In this paper, we present a numerical method to solve stochastic differential equations with PWSN. The basic idea underlying previous numerical simulations can be summarized as follows [30]. Each sample trajectory is integrated by an ordinary integration rule except at the Poisson time, at which the trajectory jumps by a random step from a prescribed distribution. In contrast, our method uses a discrete time approximation based on an integral equation which is equivalent to the stochastic differential equation. This method is similar to the Euler method widely used for systems driven by GWN [2,3], and is closely related to the method developed for dichotomous Markov noise (DMN) [31].

The paper is organized as follows. In Sec. II, we give a brief review on the existing numerical method, and present our formulation of the numerical integration scheme. In Sec. III, a comparison of the methods is presented for a particle moving in a piecewise linear periodic potential under the influence of PWSN. The paper ends with a conclusion in Sec. IV.

II. NUMERICAL METHODS

We consider the following form of a stochastic differential equation:

$$\dot{x}(t) = f(x,t) + g(x,t)\xi(t). \tag{1}$$

The random driving process $\xi(t)$ is given by PWSN which is defined as

$$\xi(t) = \sum_{k=1}^{n(t)} z_k \delta(t - \tau_k) - a, \tag{2}$$

where $\delta(t)$ is the Dirac delta function. The random times $\{\tau_k\}$ form a Poisson sequence, i.e., the probability that a sequence of k δ-impulses occurs in the interval $(0,t)$ is given by the Poissonian distribution

$$\text{Prob}\{n(t) = k\} = \frac{(\lambda t)^k e^{-\lambda t}}{k!}. \tag{3}$$

The heights $\{z_k\}$ of the δ-pulses are independent and identically distributed according to a given probability distribution $\phi(z)$. For the sake of definiteness we assume $\phi(z)$ to have an exponential distribution, even though our method is applicable for any height distribution $\phi(z)$,

$$\phi(z) = \frac{e^{-z/A}}{A}\Theta(z), \tag{4}$$

where A is the mean value of the weights and $\Theta(z)$ is the Heaviside step function. The deterministic compensator a is defined as

$$a = \lambda\langle z \rangle, \tag{5}$$

so that

$$\langle \xi(t) \rangle = 0, \tag{6}$$

where the angle brackets $\langle\ \rangle$ denote an average over realizations of the PWSN. Finally, we require that the stochastic differential equation be interpreted in the Ito sense, i.e., that the average of the random term contributing to the time rate of change in Eq. (1) vanishes,

$$\langle g(x,t)\xi(t) \rangle = 0. \tag{7}$$

We start with a brief review of the previous method used in the literature. The differences between subsequent Poissonian times $s_k = \tau_k - \tau_{k-1}$ have an exponential distribution

$$\psi(s) = \lambda e^{-\lambda s}\Theta(s), \tag{8}$$

therefore s_k can be obtained by the transformation

$$s_k = -\frac{1}{\lambda}\ln(1 - U_k) \tag{9}$$

of independent, uniformly distributed random numbers U_k from the unit interval. Analogously, random heights z_k, which are exponentially distributed according to Eq. (4), can be obtained from

$$z_k = -A\ln(1 - V_k), \tag{10}$$

where V_k is another random number having uniform distribution on the unit interval. During the times between random kicks, $\tau_{k-1} < t < \tau_k$, Eq. (1) reduces to a deterministic differential equation,

$$\dot{x}(t) = f(x,t) - ag(x,t). \tag{11}$$

At each τ_k, the impulse gives rise to a finite jump in $x(t)$. If $x(\tau_k^-)$ and $x(\tau_k^+)$ denote the values of x just before and right after the jump at τ_k, respectively, we have from Eq. (1),

$$x(\tau_k^+) = x(\tau_k^-) + z_k g^*, \tag{12}$$

where g^* represents the value of g at τ_k, whose value is determined by the integration rule applied. For the Ito rule one obtains [5,32]

$$g^* = g(x(\tau_k^-), \tau_k). \tag{13}$$

Then the value of $x(\tau_k^+)$ is determined from Eq. (12). If g does not depend on x, i.e., $g(x,t) = g(t)$, then there is no need to worry about the integration rule; g^* simply coincides with $g(\tau_k)$.

The numerical procedure to obtain $x(\tau_k^+)$ from a given value $x(\tau_{k-1}^+)$ is summarized as follows: First random numbers z_k and s_k are drawn from the probability distributions (4) and (8), respectively, next, the ordinary differential equation is numerically integrated from τ_{k-1}^+ to τ_k^- and finally $x(\tau_k^+)$ is determined by Eq. (12). This procedure can be iterated to determine a trajectory of the given stochastic differential equation for a prescribed interval of time. This method though requires variable time steps which must be adapted to each sequence of Poisson times τ_k. In particular, with increasing values of λ, the integration time step must be reduced, which causes numerical inefficiency. To cure this problem we suggest a numerical scheme that uses a constant time step. Our method is described as follows. We first draw

a random number $n(\Delta t)$ of Poisson times from the Poisson distribution, Eq. (3), and depending on that number determine the magnitude ΔX of the noise accumulated in Δt. This random increment in combination with the deterministic time evolution yields the update of the process after the time step Δt.

The method is based on the formal integration of Eq. (1) over a time step which gives

$$x(t_{n+1}) = x(t_n) + \int_{t_n}^{t_{n+1}} f(x(s),s)ds + \int_{t_n}^{t_{n+1}} g(x(s),s)\xi(s)ds,$$

(14)

where $t_{n+1}=t_n+\Delta t$. Replacing the integration time s in the functions $f(x(s),s)$ and $g(x(s),s)$ by the lower limit of integration, t_n, we have

$$x(t_{n+1}) \approx x(t_n) + f(x(t_n),t_n)\Delta t + g(x(t_n),t_n)\Delta X_n, \quad (15)$$

where the random increment ΔX_n is defined as

$$\Delta X_n = \int_{t_n}^{t_{n+1}} \xi(s)ds. \quad (16)$$

Hence we obtain the following time discrete approximation:

$$y_{n+1} = y_n + f(y_n,t_n)\Delta t + g(y_n,t_n)\Delta X_n, \quad (17)$$

where $y_0=x(t_0)$ and $y_n=y(t_n)$.

A similar form of a time discrete approximation as Eq. (17) can be found in the well-known Euler formula for an Ito process driven by the GWN [2,3], and also in the first-order truncated form of the stochastic Taylor expansion developed for the DMN [31]. However, notice that the orders of convergence of Eq. (17) are different depending on the type of noise. The order of strong convergence is 0.5 for GWN and PWSN, but 1.0 for DMN. In case of additive noise where g in Eq. (1) does not depend on x, Eq. (17) is guaranteed to be exact up to the first order in Δt for all cases of GWN, DMN, and PWSN. More detailed discussion about the convergence property of our scheme is presented in the Appendix.

For PWSN the random increment ΔX_n can be expressed by substituting Eq. (2) in Eq. (16). This yields

$$\Delta X_n = \sum_{t_n \le \tau_k < t_{n+1}} z_k - a\Delta t. \quad (18)$$

The sequence of random increments $\{\Delta X_n\}$ is defined on nonoverlapping time intervals of equal length. It therefore consists of independent identically distributed random numbers each of which is given by

$$\Delta X = \sum_{k=1}^{n(\Delta t)} z_k - a\Delta t. \quad (19)$$

The numerical procedure of our method can be summarized as follows. First determine the number of occurrences of Poisson impulses $n(\Delta t)=m$ by using Eq. (3). Next, draw m random numbers z_k from the distribution $\phi(z)$ and determine ΔX by using Eq. (19). Alternatively, if a closed expression $p(\Delta X=w)$ is known for the jump height, which is accumulated during the time step Δt, draw a random number ΔX

from this distribution. Finally, update the value of x by using Eq. (17).

The distribution of the random increment $p(\Delta X)$ can be expressed as the sum of products of two probabilities,

$$p(\Delta X = w) = \sum_{m=0}^{\infty} \text{Prob}[n(\Delta t) = m]p_m(w + a\Delta t), \quad (20)$$

where $p_m(w)dw$ is the probability that the sum of $\{z_k\}_{k=1}^m$ is between w and $w+dw$, i.e.,

$$p_m(w)dw = \text{Prob}\left(w < \sum_{k=1}^m z_k < w + dw\right) \quad (21)$$

for $m \ge 1$ and $p_0(w)=\delta(w)$. A distribution of a sum of identically distributed independent random numbers $p_m(w)$ can be represented as the m-fold convolution product of the height distribution $\phi(z)$. If $\phi(z)$ is a stable distribution then $p_m(w)$ is a rescaled version of $\phi(z)$ reading $p_m(w) = \phi(w/m)/m$. For the exponential height distribution (4) one obtains for $p_m(w)$ the Erlang distribution of order m,

$$p_m(w) = \frac{w^{m-1}e^{-w/A}}{A^m(m-1)!}\Theta(w). \quad (22)$$

Then we obtain an analytical expression of the $p(\Delta X)$ from Eqs. (3), (20), and (22) as follows:

$$p(\Delta X = w) = e^{-\lambda\Delta t}\left(\delta(w + a\Delta t) + \Theta(w + a\Delta t)\right.$$

$$\left. \times \sum_{k=1}^{\infty} \frac{(\lambda\Delta t)^k(w + a\Delta t)^{k-1}e^{-(w+a\Delta t)/A}}{(k-1)! \, k! \, A^k}\right).$$

(23)

We give an alternative derivation of this result based on the integral of the PWSN as a function of the upper integration limit

$$X(t) = \int_0^t \xi(u)du. \quad (24)$$

This process is Markovian. The probability density $q(z,t)$ to find $X(t)=z$ satisfies the following integro-differential equation [7]:

$$\frac{\partial}{\partial t}q(z,t) = a\frac{\partial}{\partial z}q(z,t) + \lambda\int_{-\infty}^{\infty} \phi(y)[q(z-y,t) - q(z,t)]dy,$$

(25)

with initial condition $q(z,0)=\delta(z)$. Since $p(\Delta X=w)$ is equal to $q(w,\Delta t)$, we can obtain an analytical expression for $p(\Delta X)$ by solving Eq. (25). The characteristic function

$$\tilde{q}(u,t) = \int_{-\infty}^{\infty} q(z,t)e^{iuz}dz \quad (26)$$

satisfies the first-order differential equation

$$\frac{\partial}{\partial t}\tilde{q}(u,t) = \{-iau + \lambda[\tilde{\phi}(u) - 1]\}\tilde{q}(u,t), \qquad (27)$$

with initial condition $\tilde{q}(u,0)=1$. Here $\tilde{\phi}(u)$ denotes the characteristic function of the height distribution

$$\tilde{\phi}(u) = \int_{-\infty}^{\infty} \phi(z)e^{iuz}dz. \qquad (28)$$

Equation (27) is readily solved for $\tilde{q}(u,t)$ to yield [28]

$$\tilde{q}(u,t) = \exp(\{-iau + \lambda[\tilde{\phi}(u) - 1]\}t). \qquad (29)$$

For the exponential height distribution (4), $q(z,t)$ becomes

$$q(z,t) = e^{-\lambda t}\delta(z+at) + \sum_{k=1}^{\infty} \frac{(\lambda t)^k e^{-\lambda t}}{k!}\frac{(z+at)^{k-1}e^{-(z+at)/A}}{A^k(k-1)!}$$
$$\times \Theta(z+at). \qquad (30)$$

Thus we retrieve the analytical expression of $p(\Delta X)$ obtained from Eq. (23) above.

In the limit

$$\lambda \to \infty, \quad A \to 0 \quad \text{with } \lambda A^2 = D \text{ fixed}, \qquad (31)$$

PWSN approaches GWN, cf. Ref. [7]. Performing this limit for $q(z,t)$ in Eq. (30) we find the correct Gaussian distribution for the increments of the Wiener process with fixed time step Δt, i.e.,

$$p(\Delta X = w) = \frac{1}{\sqrt{4\pi D\Delta t}}\exp\left(-\frac{w^2}{4D\Delta t}\right). \qquad (32)$$

Therefore, the integration scheme also reduces to the Euler form [2,3] in the limit of GWN.

III. NUMERICAL EXAMPLE

To check the accuracy and the efficiency of our method, we performed a numerical simulation for a system composed of an ensemble of noninteracting particles, each of which is driven by PWSN in a spatially periodic potential [14,15]. We calculated the stationary probability distribution and the probability current with periodic boundary conditions, as well as the effective drift and the effective diffusion coefficient with natural boundary conditions. The simulated results were compared with the numerical results obtained from the analytical expressions. We further demonstrate that our method also works in the opposite asymptotic limits of Gaussian white noise and strong collisions.

The dynamics of the system is described by a Langevin equation with additive noise of the form

$$\dot{x}(t) = -V'(x) + \xi(t), \qquad (33)$$

where $V(x)$ is a spatially periodic potential with period L, i.e., $V(x+L)=V(x)$. The specific form of the potential for the numerical simulation is assumed as

$$V(x) = |x| \quad \text{if } -\frac{1}{2}L \le x < \frac{1}{2}L. \qquad (34)$$

The random force $\xi(t)$ is the PWSN as defined in Eq. (2) with exponentially distributed weights obeying Eq. (4). Thus the deterministic compensator is given as

$$a = \lambda A \qquad (35)$$

and the noise strength as

$$D = \lambda A^2. \qquad (36)$$

If we use D and λ as noise parameters, a is given as $\sqrt{D\lambda}$ and A as $\sqrt{D/\lambda}$.

Two stochastic processes which differ by their respective boundary conditions were considered: One process, $x(t)$, satisfies natural boundary conditions, and the other one, $\hat{x}(t)$, fulfills periodic boundary conditions. With natural boundary conditions the state space of the process $x(t)$ evolving according to Eq. (33) is the whole real axis. In this case the numerical scheme discussed in the preceding section can be implemented without modification. For periodic boundary conditions, the process $\hat{x}(t)$ is restricted to a unit cell of the potential $V(x)$, i.e., to the interval $I=[-L/2,L/2)$,

$$-\frac{1}{2}L \le \hat{x}(t) < \frac{1}{2}L. \qquad (37)$$

Once the process leaves this interval through either boundary it is reset into the interval through the other boundary. Within the numerical scheme one must control after each integration step whether the process has left the interval. If this is the case, an integral multiple of L must be added or subtracted such that the resulting value lies in I.

The process with natural boundaries is nonstationary. It is characterized by an effective drift and an effective diffusion coefficient, which are defined as

$$U_{\text{eff}} = \lim_{t\to\infty}\frac{\langle x(t)\rangle}{t} \qquad (38)$$

and

$$D_{\text{eff}} = \lim_{t\to\infty}\frac{\langle x^2(t)\rangle - \langle x(t)\rangle^2}{2t}, \qquad (39)$$

respectively. In contrast to the process with natural boundary conditions, the process with periodic boundary conditions becomes stationary in the limit of long times. The corresponding stationary probability density $\hat{p}_{\text{st}}$ is defined as

$$\hat{p}_{\text{st}}(x) = \lim_{t\to\infty}\langle\delta(x - \hat{x}(t))\rangle. \qquad (40)$$

In general, this stationary state carries a probability current J_{st}, which is independent of the position $x \in I$ and related to the velocity in this stationary state

$$\langle\dot{\hat{x}}\rangle_{\text{st}} = LJ_{\text{st}}. \qquad (41)$$

The stationary probability density and current satisfy the following differential equation, which was obtained by Łuczka *et al.* [14]:
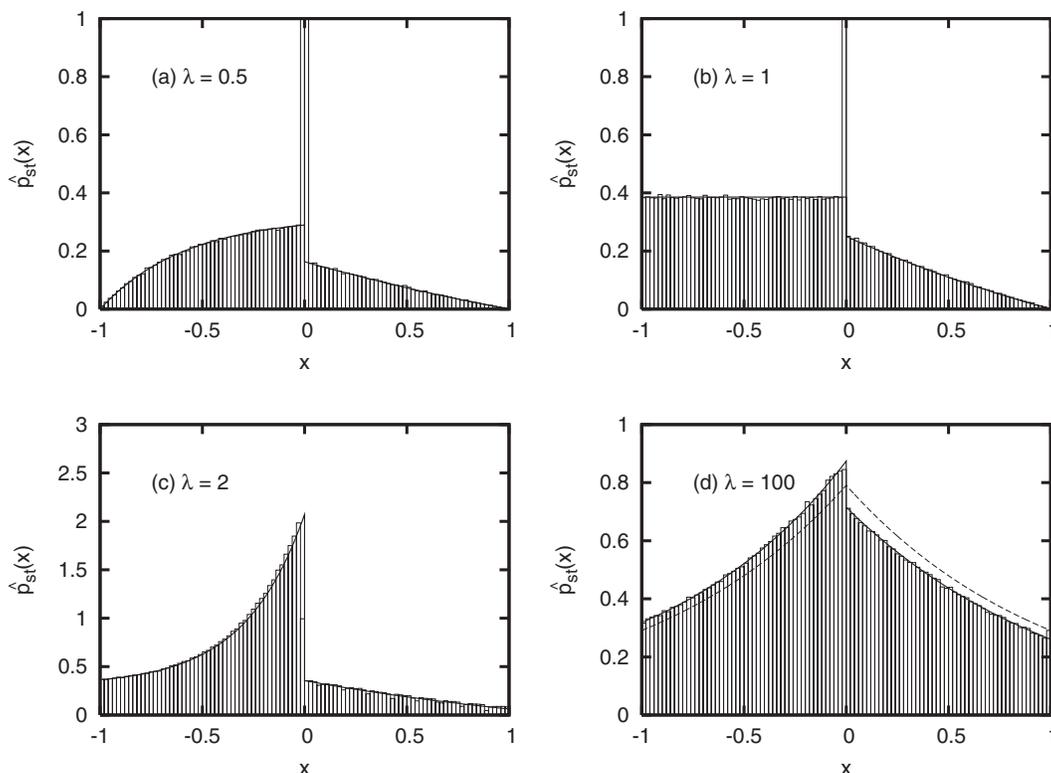
FIG. 1. Stationary distributions $\hat{p}_{st}(x)$ for the process $\hat{x}(t)$. The numerical results obtained by using our numerical method are represented as histograms and the analytical results are depicted as solid lines. The noise strength is set to $D=1$ and four values of λ are used: (a) $\lambda =0.5$ (nondiffusive regime), (b) $\lambda=1$ (transition point), (c) $\lambda=2$ (diffusive regime), and (d) $\lambda=100$ (near the GWN limit). The dashed line in (d) represents the stationary distribution in the GWN limit.

$$A\{[V'(x) + \lambda A]\hat{p}_{st}(x)\}' + V'(x)\hat{p}_{st}(x) + J_{st} = 0. \quad (42)$$

The value of J_{st} is determined by the periodic boundary condition $\hat{p}(-L/2)=\hat{p}(L/2)$ and normalization $\int_{-L/2}^{L/2}dx\hat{p}(x)=1$. The analytical forms of the solutions $\hat{p}_{st}$ and J_{st} for the case of a piecewise linear potential covering the entire range of the noise parameter space (D,λ) have been presented in Ref. [15].

The above-mentioned characteristic quantities of the two processes $x(t)$ and $\hat{x}(t)$ were determined from respective N trajectories in the following way. The numerical values of U_{eff} and D_{eff} were obtained from estimates of the moments $\langle x(t)\rangle$ and $\langle x^2(t)\rangle$, respectively, by using Eqs. (38) and (39). The stationary distribution $\hat{p}_{st}(x)$ was estimated from a histogram of the values which the N simulated trajectories $\hat{x}(t)$ take at the final time T. The stationary current was determined from the numbers n_R and n_L which count how often the right and left boundaries, respectively, were crossed. Jumps to the nth next period within one time step increase either n_R or n_L by n depending on the direction of the jump to the right or to the left, respectively. The probability current finally is given by

$$J_{st} = \frac{n_R - n_L}{NT}. \quad (43)$$

Throughout the numerical simulations, the length of one period of the periodic potential and the integration time step were fixed as $L=2$ and $\Delta t=0.01$, respectively. The number of samples N and the length of the time T were chosen sufficiently large to get statistically reliable results. For the calculation of U_{eff} and D_{eff}, a number of 10^6 trajectories of $x(t)$ was generated with fixed $T=10$. For the calculation of $p_{st}(x)$ and the probability current J_{st}, the same number of sample trajectories of lengths $T=10^2$ and $T=10^3$, respectively, was simulated. For comparison, numerical integrations by using the previous method were performed under the same conditions. The Euler method was employed to integrate the deterministic equation (11). The grid points were chosen as the union of the set of the Poissonian times $\{\tau_k\}$ and the equidistant times $\{t_n=n\Delta t\}$. If the next integration point is one of the Poissonian times, an update of the trajectory due to the impulse [see Eq. (12)] follows the Euler integration.

Figure 1 shows the stationary distributions of a Brownian particle whose dynamics is governed by Eq. (33). The numerical results obtained by our method and the analytical solution of Ref. [15] are depicted as histograms and as solid lines, respectively. In this comparison, the noise strength was fixed at $D=1$, while four different values of λ were employed to observe the change of the stationary distribution as the system transits from a nondiffusive to a diffusive regime [15]. Although a transition over a barrier of the periodic potential to the positive direction is always possible due to the positive δ spikes of the shot noise, the backward movement is possible only when the deterministic compensator a is large enough to overcome the barrier. If the noise activates
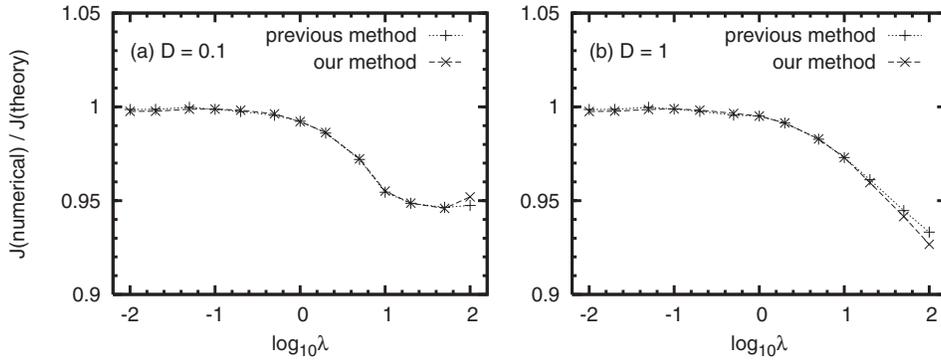
FIG. 2. The ratios of the numerical and analytical values of the stationary current are plotted. The values obtained from our method and the previous method are plotted as diagonal crosses and upright crosses, respectively. Two values of the noise strength are used, (a) $D=0.1$ and (b) 1.

movements over the barriers in both directions, the system is referred to as being in the diffusive, otherwise in the nondiffusive regime. In the nondiffusive regime, $\hat{p}_{st}(x)$ contains a δ-peak at the local minimum of the potential, because the Brownian particle stays there waiting for the next δ spike with finite probability. The numerical results in Fig. 1 show excellent agreement with the analytical results. They clearly exhibit the transition from the nondiffusive to the diffusive regime as the value of λ changes. In the limit of the GWN [see Eq. (31)], $\hat{p}_{st}(x)$ approaches the equilibrium Boltzmann distribution,

$$\hat{p}_{st}(x) = Z^{-1} e^{-V(x)/D}, \quad (44)$$

where Z^{-1} is a normalization constant. This limiting behavior is shown in Fig. 1 for comparison.

The accuracy of our numerical method was tested by comparing the numerically obtained stationary currents with the analytical results for a wide range of λ values [15]. The errors of the numerical values of the stationary currents computed by our method and by the previous method are compared in Fig. 2. The previous method allows for the finite jumps in x at exactly the times when the δ pulses take place, whereas our method approximates the impacts by the accumulated effect of a sequence of pulses during a given time interval. So one would expect that the previous method generated more accurate results. Still, the two methods produce nearly the same size of error, cf. Fig. 2. The errors of both

methods grow as λ increases, because then the system becomes more stiff. The computation times needed for the two methods are compared in Fig. 3 for the same time step $\Delta t = 0.01$. In both cases, they depend on the value of λ but not on the value of D. For small values $\lambda < 1$, both methods require almost the same amount of computation times, which are almost insensitive to the value of λ. Only if λ increases above the value of 1, then both methods require more computation times. The previous method though slows down more drastically. At $\lambda = 100$ the previous method requires about 2 times as much computation time.

Figure 4 presents a comparison of the velocities U_{eff} and $\langle \dot{x} \rangle_{st}$, together with analytical results based on the stationary probability current [15] for various values of λ ranging from 10^{-2} to 10^2 with three values of $D=0.1$, 0.5, and 1. The figure corroborates that our method provides reasonably accurate numerical results over a wide range of λ and D. From the figure, the effective drift U_{eff} and the stationary velocity $\langle \dot{x} \rangle_{st}$ apparently coincide with each other within the graphical resolution. Thus the following relation can be conjectured:

$$U_{eff} = L J_{eff}. \quad (45)$$

This can be confirmed by the following arguments, cf. also Ref. [33]. If the two processes $x(t)$ and $\hat{x}(t)$ start from the
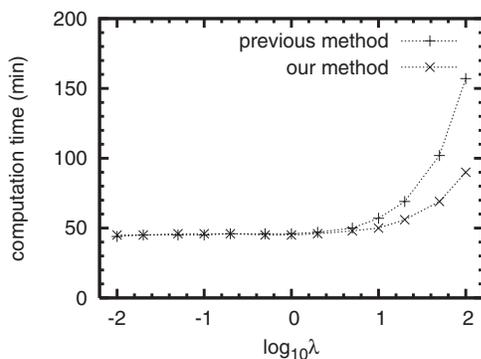

FIG. 3. The computation time needed for 10^6 trajectories of length $T=10^2$ as a function of the Poisson parameter λ is depicted for the previous method and our method. For large values of λ our method becomes faster than the previous one.
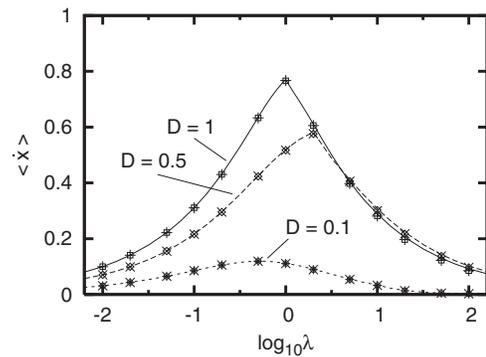

FIG. 4. The stationary velocity $\langle \dot{x} \rangle_{st}$ and the effective drift U_{eff} are depicted as functions of the logarithm of the Poisson parameter λ for three different values of the noise intensity. The stationary velocities obtained by using our method are indicated as empty circles, diamonds, and squares; the analytical results are given as dotted, dashed, and solid lines, and the effective drifts obtained by our method are presented by asterisks, diagonal crosses, and upright crosses, for $D=0.1$, 0.5, and 1, respectively.
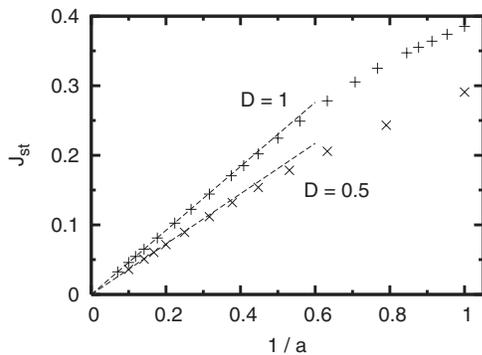
FIG. 5. Plots of the stationary current J_{st} versus the inverse of deterministic compensator a for large values of a. The numerical results for $D=0.5$ and 1 are depicted as diagonal crosses and upright crosses, respectively. The asymptotes are also plotted as dashed lines.

same value, they remain related to each other by an integer multiple of the period L,

$$\hat{x}(t) = x(t) - Ln(t), \tag{46}$$

where $n(t)$ is an integer such that $\hat{x} \in I$, i.e., $n(t)$ is the integer which is next to $x(t)/L$. Thus, $n(t)$ indicates the net number of the period boundaries that the particle has crossed in forward direction up to the time t. If we substitute Eq. (46) into Eq. (38) and use Eq. (37), we have

$$U_{\mathrm{eff}} = L \lim_{t \to \infty} \frac{\langle n(t) \rangle}{t}. \tag{47}$$

On the other hand, the stationary probability current J_{st} equals the averaged net number of periods the process proceeds per time, i.e.,

$$J_{st} = \lim_{t \to \infty} \frac{\langle n(t) \rangle}{t}. \tag{48}$$

We note that Eq. (43) is based on an estimate of the mean value $\langle n(t) \rangle$ entering Eq. (48). From Eqs. (47) and (48), Eq. (45) is obtained.

We also examined the accuracy of our method in the limits of large and small parameters a with the constant $D=aA$ fixed. In the first case, $a \to \infty$, the PWSN approaches GWN as stated in Eq. (31). In this limit the symmetry of detailed balance which is a characteristic feature of an equilibrium state is restored with the consequence that the probability current vanishes. The current approaches this limit inversely proportional to a, cf. Ref. [14],

$$J_{st}(a \to \infty) = \frac{e^{1/D}}{2aD^2(e^{1/D}-1)^2} + O(1/a^2). \tag{49}$$

In Fig. 5, the current J_{st} is plotted against the inverse of the deterministic compensator a for two different values of the noise intensity $D=0.5$ and 1. As the value of a becomes large, our numerical results approach the asymptotic behavior which is predicted by Eq. (49).

In the other limiting case a approaches zero with D fixed. This strong collision limit is obtained by taking $\lambda \to 0$ and
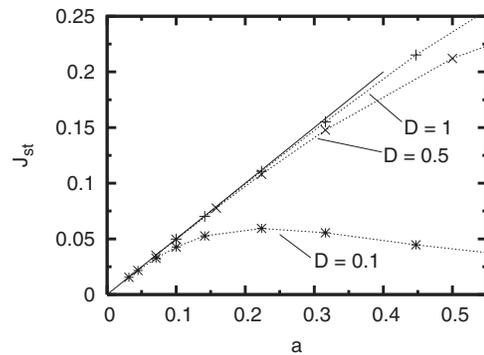

FIG. 6. Plots of the stationary current J_{st} versus the deterministic compensator a for small value of a. The numerical values of J_{st} are indicated as asterisks, diagonal crosses, and upright crosses for the noise intensity $D=0.1$, 0.5, and 1, respectively, together with dotted lines as a guide for the eyes. The asymptote is plotted as the solid line.

$A \to \infty$ simultaneously. In this limit, the occurrences of δ pulses become very rare, while the average value of the pulse amplitudes becomes very large. As the amplitude of the δ pulses becomes much larger compared to the spatial period of the potential, i.e., $L \ll A$, the influence of the potential on the motion of the particle becomes negligible. Therefore, the motion of the particle can be well described by the following simple equation:

$$\dot{x}(t) = \widetilde{\xi}(t), \tag{50}$$

where $\widetilde{\xi}(t)$ is the PWSN described as

$$\widetilde{\xi}(t) = \sum_{k=1}^{n(t)} z_k \delta(t - \tau_k), \tag{51}$$

which is without the deterministic compensator term. Then, the motion is strictly biased to the positive direction. In this limit the average and the variance of $x(t)$ are given by

$$\langle x(t) \rangle = at, \tag{52}$$

$$\langle x^2(t) \rangle - \langle x(t) \rangle^2 = 2Aat. \tag{53}$$

From Eqs. (38), (45), and (52), the stationary current in this limit becomes simply

$$J_{st}(a \to 0) \approx \frac{a}{L}. \tag{54}$$

In Fig. 6 the current J_{st} is depicted as a function of a for three different values of the noise intensity $D=0.1$, 0.5, and 1, together with the asymptote given in Eq. (54). While the asymptote itself is independent of the noise strength D, the region where the current follows the asymptotic behavior shrinks with decreasing noise strength D. Since the mean amplitude A is proportional to the noise strength D for fixed value of a, cf. Eqs. (35) and (36), a particle with larger D is expected to perform wider jumps. Accordingly, the current approaches the asymptotic behavior (54) provided the condition $L \ll A$ is satisfied.
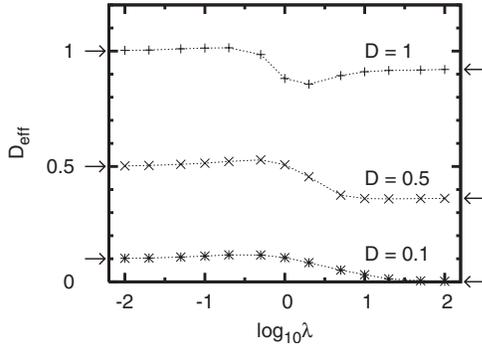
FIG. 7. Plots of the effective diffusion coefficient D_{eff} versus the logarithm of λ. The numerical results are represented by asterisks, diagonal crosses, and upright crosses for the noise intensity D =0.1, 0.5, and 1, respectively, together with dotted lines as a guide for the eyes. The arrows on the left-hand and right-hand side of the graph point to the values in the asymptotic limit of D_{eff} as $\lambda \rightarrow 0$ and $\lambda \rightarrow \infty$, respectively.

Figure 7 represents the effective diffusion coefficient D_{eff} as a function of the logarithm of the Poisson parameter λ ranging from 10^{-2} to 10^{2} for three different values of the noise intensity D=0.1, 0.5, and 1. The asymptotic values of D_{eff} for the cases where λ goes to 0 or infinity are indicated by the arrows in Fig. 7. In the GWN limit, D_{eff} can be given as [34,35]

$$D_{\text{eff}} = \frac{e^{1/D}}{D(1 - e^{1/D})^2}. \tag{55}$$

On the other hand, it follows from Eqs. (39) and (53), that for $\lambda \rightarrow 0$, D_{eff} becomes

$$D_{\text{eff}} = D. \tag{56}$$

IV. CONCLUSION

In this paper, we presented a numerical integration method for solving stochastic differential equations with PWSN. In contrast to the previous method, which is based on the simulation of Poisson sequences of pulses, our method introduces a random increment ΔX which samples the effect of all random pulses acting within a fixed time step Δt, cf. Eq. (16). The analytical form of the probability distribution of ΔX was obtained for exponentially distributed pulse strengths. We also demonstrated that our numerical scheme approaches the Euler scheme for the GWN limit in a smooth manner. To examine the accuracy and efficiency of our method, we investigated the motion of an overdamped particle in a piecewise linear periodic potential driven by PWSN with natural and periodic boundary conditions. For this model analytic results are known in the literature. We compared the stationary probability density in the presence of periodic boundary conditions as well as the average velocity and the effective diffusion constant obtained with our method both with analytical results and numerical simulations performed with the previous method. We observed that our method maintains reasonably good accuracy over a wide

parameter range, regardless of whether the system is in the diffusive or nondiffusive regime, and shows a higher efficiency than the previous method especially when the value of λ becomes large. Our method also faithfully reproduces the known asymptotic behavior both in the GWN limit and in the strong collision limit.

APPENDIX

Equation (1) can be written as follows:

$$dx(t) = \tilde{f}(x,t)dt + g(x,t)dN_t, \tag{A1}$$

where

$$\tilde{f}(x,t) = f(x,t) - ag(x,t). \tag{A2}$$

Here N_t is the compound Poissonian process defined as

$$N_t = \sum_{k=1}^{n(t)} z_k \Theta(t - \tau_k) \tag{A3}$$

and dN_t is the infinitesimal increment defined as

$$dN_t = N_{t+dt} - N_t. \tag{A4}$$

The Ito formula applied to Eq. (A1) can be written in the differential form as follows [5,32]:

$$dh(x(t),t) = [\dot{h}(x(t),t) + h'(x(t),t)\tilde{f}(x(t),t)]dt$$
$$+ \{h[x(t) + g(x(t),t)dN_t,t] - h(x(t),t)\}, \tag{A5}$$

where an overdot denotes a partial differentiation with respect to time and a prime denotes differentiation with respect to the state variable x. Equation (A5) is equivalent to the following integrated form:

$$h(x(t),t)$$
$$= h(x(s),s) + \int_s^t [\dot{h}(x(u),u) + h'(x(u),u)\tilde{f}(x(u),u)]du$$
$$+ \sum_{s \le \tau_k < t} \{h[x(\tau_k^-) + z_k g(x(\tau_k^-),\tau_k),\tau_k] - h(x(\tau_k^-),\tau_k)\}. \tag{A6}$$

By applying Eq. (A6) to Eq. (14), Eq. (15) is recovered if the remainder is ignored. Successive application of the Ito formula to this remainder develops systematically higher-

order approximation forms. Hence, it forms a hierarchical set, and Eq. (15) corresponds to the first order in the set.

To examine the convergence property of our numerical scheme, let us consider the root-mean-square error between the sample path of the process $x(t)$ and the approximation $y(t)$ at the final time T,

$$\epsilon = \langle |x(T) - y(T)|^2 \rangle^{1/2}. \tag{A7}$$

Then, the rate of the convergence γ can be estimated from the following inequality which determines the behavior of $\epsilon(\Delta t)$ as a function of time step Δt:

$$\epsilon(\Delta t) = \langle |x(T) - y_{\Delta t}(T)|^2 \rangle^{1/2} \leq C(\Delta t)^\gamma, \tag{A8}$$

where C is a constant, and $y_{\Delta t}(t)$ is the approximation of $x(T)$ for a finite time step Δt.

From Eqs. (14) and (17), we have

$$x(t_n) - y_n = x(t_{n-1}) - y_{n-1} + I_n^{(1)} + I_n^{(2)} + I_n^{(3)} + I_n^{(4)}, \tag{A9}$$

where

$$I_n^{(1)} = \int_{t_{n-1}}^{t_n} [f(x(s),s) - f(x(t_{n-1}),t_{n-1})]ds, \tag{A10}$$

$$I_n^{(2)} = \int_{t_{n-1}}^{t_n} [g(x(s),s) - g(x(t_{n-1}), t_{n-1})]\xi(s)ds, \tag{A11}$$

$$I_n^{(3)} = [f(x(t_{n-1}),t_{n-1}) - f(y_{n-1},t_{n-1})]\Delta t, \tag{A12}$$

$$I_n^{(4)} = [g(x(t_{n-1}),t_{n-1}) - g(y_{n-1},t_{n-1})]\Delta X_{n-1}. \tag{A13}$$

From Eq. (A9), the difference between $x(t)$ and $y(t)$ at the final time $T = t_M$ is expressed as follows:

$$x(t_M) - y_M = \sum_{n=1}^{M} (I_n^{(1)} + I_n^{(2)} + I_n^{(3)} + I_n^{(4)}). \tag{A14}$$

Hence, the root-mean-square error ϵ is expressed in terms of $I_n^{(k)}$. Under the Lipshitz conditions and the linear growth conditions, which are generally assumed to hold for the functions f and g in Eq. (1), the stochastic differential equation admits a unique solution [32]. Then the expectations of $I_n^{(k)} I_m^{(j)}$
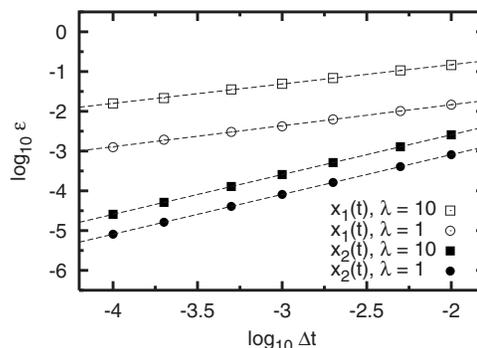

FIG. 8. Plots of the logarithm of the root-mean-square error ϵ versus the logarithm of time step Δt. The numerical results of the ϵ for the processes $x_1(t)$ and $x_2(t)$ are displayed for $\lambda=1$ [empty circles for $x_1(t)$, and filled circles for $x_2(t)$] and $\lambda=10$ [empty squares for $x_1(t)$, and filled squares for $x_2(t)$], respectively. The dashed lines represent linear fits to the data.

can be estimated by applying the Ito formula and the rate of convergence γ in this case is known as 0.5. When the noise is additive, i.e., $g(x,t)=g(t)$, the rate increases up to $\gamma=1$. A rigorous mathematical proof for the convergence problems in general is given in Ref. [36].

We present results of numerical studies of the root-mean-square errors for the following two linear stochastic differential equations:

$$\dot{x}_1(t) = x_1(t)\xi(t), \tag{A15}$$

$$\dot{x}_2(t) = -x_2(t) + \xi(t), \tag{A16}$$

where $\xi(t)$ is the PWSN defined in Eq. (2). Then the analytic solutions are available for both $x_1(t)$ and $x_2(t)$.

The root-mean-square errors ϵ were calculated for various time steps ranging from 10^{-2} to 10^{-4} with $T=0.01$. The mean height of impulses was set as $A=1$ and the Poisson parameter λ was chosen as 1 and 10. Total number of 10^9 sample trajectories were generated for each simulation. Figure 8 shows a log-log plot of error ϵ versus time step Δt. The slopes for process $x_1(t)$ and process $x_2(t)$ were observed to be 0.5 and 1, respectively, which confirm the theoretical predictions.

[1] H. Risken, *The Fokker-Planck Equation* (Springer-Verlag, Berlin, 1984).

[2] C. W. Gardiner, *Handbook of Stochastic Methods*, 3rd ed. (Springer-Verlag, Berlin, 2004).

[3] P. E. Kloeden and E. Platen, *Numerical Solution of Stochastic Differential Equations* (Springer-Verlag, Berlin, 1992).

[4] P. Hänggi, Z. Phys. B **31**, 407 (1978).

[5] P. Hänggi, Z. Phys. B **36**, 271 (1980).

[6] P. Hänggi, K. E. Shuler, and I. Oppenheim, Physica A **107**, 143 (1981).

[7] C. Van Den Broeck, J. Stat. Phys. **31**, 467 (1983).

[8] B. J. West, K. Lindenberg, and V. Seshadri, Physica A **102**,

470 (1980).

[9] P. Hänggi, Phys. Lett. **A78**, 304 (1980).

[10] N. G. Van Kampen, Physica A **102**, 489 (1980).

[11] F. X. Barcons and L. Garrido, Physica A **117**, 212 (1983).

[12] A. Taloni and F. Marchesoni, Phys. Rev. Lett. **96**, 020601 (2006).

[13] F. Marchesoni and A. Taloni, Phys. Rev. Lett. **97**, 106101 (2006).

[14] J. Łuczka, R. Bartussek, and P. Hänggi, Europhys. Lett. **31**, 431 (1995).

[15] T. Czernik and J. Łuczka, Ann. Phys. **9**, 721 (2000).

[16] P. Hänggi, R. Bartussek, P. Talkner, and J. Łuczka, Europhys.

Lett. **35**, 315 (1996).

[17] P. Reimann, Phys. Rep. **361**, 57 (2002).

[18] T. Czernik, J. Kula, J. Łuczka, and P. Hänggi, Phys. Rev. E **55**, 4057 (1997).

[19] J. Łuczka, T. Czernik, and P. Hänggi, Phys. Rev. E **56**, 3968 (1997).

[20] P. D. Ditlevsen, Geophys. Res. Lett. **26**, 1441 (1999).

[21] R. Metzler and J. Klafter, Phys. Rep. **339**, 1 (2000).

[22] A. V. Chechkin, V. Yu. Gonchar, J. Klafter, and R. Metzler, Europhys. Lett. **72**, 348 (2005).

[23] B. Dybiec, E. Gudowska-Nowak, and P. Hänggi, Phys. Rev. E **73**, 046104 (2006); **75**, 021109 (2007).

[24] R. Zygadło, Phys. Lett. A **329**, 459 (2004).

[25] M. A. Rodriguez, L. Pesquera, M. San Miguel, and J. M. Sancho, J. Stat. Phys. **40**, 669 (1985).

[26] J. M. Sancho, M. San Miguel, L. Pesquera, and M. A. Rodriguez, Physica A **142**, 532 (1987).

[27] C. Van den Broeck and P. Hänggi, Phys. Rev. A **30**, 2730 (1984); P. Hänggi and P. Talkner, *ibid.* **32**, 1934 (1985); J.

Masoliver, *ibid.* **35**, 3918 (1987); E. Hernández-Garcia, L. Pesquera, M. A. Rodriguez, and M. San Miguel, *ibid.* **36**, 5774 (1987); J. M. Porrà and J. Masoliver, Phys. Rev. E **47**, 1633 (1993); F. Laio, A. Porporato, L. Ridolfi, and I. Rodriguez-Iturbe, *ibid.* **63**, 036105 (2001).

[28] E. Daly and A. Porporato, Phys. Rev. E **73**, 026108 (2006).

[29] R. Zygadło, Phys. Rev. E **47**, 106 (1993).

[30] R. Mikulevicius and E. Platen, Math. Nachr. **138**, 93 (1988).

[31] C. Kim, E. K. Lee, and P. Talkner, Phys. Rev. E **73**, 026101 (2006).

[32] I. I. Gihman and A. V. Skorokhod, *Stochastic Differential Equations* (Springer-Verlag, Berlin, 1972).

[33] L. Machura, M. Kostur, F. Marchesoni, P. Talkner, P. Hänggi, and J. Łuczka, J. Phys.: Condens. Matter **17**, S3741 (2005).

[34] S. Lifson and J. L. Jackson, J. Chem. Phys. **36**, 2410 (1962).

[35] R. Festa and E. Galleani d'Agliano, Physica A **90**, 229 (1978).

[36] N. Bruti-Liberati and E. Platen, Technical Report, University of Technology, Sydney, QFRC Research Paper 157, 2005.